Journal of Digital Imaging

Novel Computer-Aided Diagnosis Algorithms on Ultrasound Image: Effects on Solid Breast Masses Discrimination

Ying Wang,[1] Hong Wang,[1] Yanhui Guo,[2] Chunping Ning,[1] Bo Liu,[2] H. D. Cheng,[2,3] and Jiawei Tian[1]

The objective of this study is to retrospectively investigate whether using the newly developed algorithms would improve radiologists' accuracy for discriminating malignant masses from benign ones on ultrasonographic (US) images. Five radiologists blinded to the histological results and clinical history independently interpreted 226 cases according to the sonographic lexicon of the fourth edition of the Breast Imaging Reporting and Data System and assigned a final assessment category to indicate the probability of malignancy. For each case, each radiologist provided three diagnoses: first with the original images, subsequently with the assistant of the resulting images processed by the proposed CAD algorithms which are called as processed images, and another using the processed images only. Observers' malignancy rating data were analyzed with the receiver operating characteristic (ROC) curve. For reading only with the processed images, areas under the ROC curve (A_z) of each reader (0.863, 0.867, 0.859, 0.868, 0.878) were better than that with the original images (0.772, 0.807, 0.796, 0.828, 0.846), difference of the average A_z between the twice reading was significant ($p<0.001$). Compared with the results single used processed images, A_z of utilizing the combined images were increased (0.866, 0.885, 0.872, 0.894, 0.903), but the difference is not statistically significant ($p = 0.081$). The proposed CAD method has potential to be a good aid to radiologists in distinguishing malignant breast solid masses from benign ones.

KEY WORDS: Computer-aided diagnosis, ultrasound, breast cancer, BI-RADS

INTRODUCTION

Breast cancer is still one of the most common cancers and a leading cause of death among women.[1,2] Early detection and diagnosis are essential in reducing the mortality and improving the clinical curative rate and life quality of patients. Mammography has been a preferred method for breast cancer detection. Although the role of mammography for early detection of breast cancer is well recognized, mammography is very sensitive but not specific to detecting breast cancer; it also has limitations on cancer detection of dense breasts of young patients.[3]

Sonography plays an important role in differentiating cysts from solid breast masses and is helpful in reducing the negative biopsy ratio. There is growing evidence that it can detect clinically and mammographically occult cancers. Also, it is now a key mode of imaging for the clinical diagnosis of breast cancer. A standardized lexicon for sonography, Breast Imaging Reporting and Data System (BI-RADS) for US was developed in 2003 by the American College of Radiology.[4] It has been proven that sonographic features introduced by the BI-RADS were useful in distinguishing malignant masses from benign ones.[5,6] But the diagnosis accuracy depends mostly upon the quality of images and the experience of radiologists. In order to further improve the performance, many computer-aided analysis methods have been developed.[7–12] Shen et

[1]*From the Ultrasound Department, The Second Affiliated Hospital of Harbin Medical University, 246 Xuefu Road, Harbin, Heilongjiang 150086, People's Republic of China.*

[2]*From the School of Computer Science and Technology, Harbin Institute of Technology, Harbin 150001, China.*

[3]*From the Department of Computer Science, Utah State University, Logan, UT 84322, USA.*

Correspondence to: Jiawei Tian, Ultrasound Department, The Second Affiliated Hospital of Harbin Medical University, 246 Xuefu Road, Harbin, Heilongjiang 150086, People's Republic of China; tel: +86-451-86605811; fax: +86-451-86675845; e-mail: jwtian2004@yahoo.com.cn

Online publication 10 November 2009

doi: 10.1007/s10278-009-9245-1

al. quantified all feature classes defined in the BI-RADS into eight computerized features and developed a classification system of breast lesions. They pointed out that the advantage for CAD system using the BI-RADS features is that the CAD system could be applied on different ultrasound systems.[8] Chen et al. developed a CAD algorithm with setting-independent features and artificial neural networks to differentiate benign from malignant breast lesions.[9] Huang et al. also developed a CAD algorithm using morphological features for classifying breast lesions on ultrasound,[10] and there are other experiments placed on the 3D US volumetric images for Classification.[11,12] In these studies, computers are trained to assign a probability of malignancy, and the outputs were provided to the radiologists as a second opinion for breast mass discrimination. The previous studies showed the possibility of CAD in automatic classification of breast lesion, but the computerized features and outputs are always not intuitive for lesion interpretation and radiologists' diagnosis. To better display the BI-RADS sonographic features and provide more visible, easily understandable, and acceptable information for radiologists, we developed a CAD method to delineate mass boundaries and enhance the textures of the images. This study focuses on validating the effectiveness and usefulness of the proposed computer-aided diagnosis approach by clinical trials.

MATERIALS AND METHODS

Image Database

Informed consent to the protocol was obtained from all patients in this study. The study protocol was approved by the Institutional Ethics Committee of Harbin Medical University for human research. Our experimental database consists of 226 female patients (mean age ± SD, 43.20± 11.43 years; range, 21–75 years) who underwent breast ultrasound examinations in the Second Affiliated Hospital of Harbin Medical University, Dec. 22, 2002 and Jan. 20, 2008. A total of 839 ultrasound images of 226 pathology-proven cases were analyzed. Because of a high diagnosis rate for cystic lesions, even close to 100% by experienced breast radiologists,[13] cystic lesions were excluded in this study. On the basis of surgical excision or US-guided percutaneous core-needle biopsy findings, 106 (46.9%) masses were classified as benign and 120 (53.1%) were classified as malignant.

Ultrasonographic Examinations

All the sonography explorations were performed by a radiologist with more than 10 years experience in breast US. A Vivid 7 system (GE Healthcare, Milwaukee, WI) equipped with a 5.6–14 MHz linear-array transducer that has 38-mm scan width was used.

Conventional ultrasonography was performed on the patients in the supine position with double breasts exposed fully or lateral decubitus position if the lesions were on the lateral of the breast. Both breasts were scanned directly and compared with each other. The ultrasound characteristics of lesions were obtained. The lesions were scanned along different directions and angles, and the occipitofrontal, transverse, and up–down diameters were measured.

Representative views of a lesion, a suspected lesion, or normal tissue were digitally recorded from the frozen images, and all images were saved in the database for double-blind analysis. One to nine images were obtained from each mass, and there was only one mass in each image.

Image Processing

Enhancement

At first, a region of interest (ROI) is manually selected by the radiologist from the full breast ultrasound image (Fig. 1). Define the ROI in the full breast ultrasound image as I_{ori}. In this study, the radiologist selects the ROI using software developed by ourselves. The brief description about the enhancement algorithm is as following. Firstly, the images are normalized by mapping the intensity levels into a desired range. Secondly, the images are fuzzified. The standard S function was used as a suitable membership function.[14] The maximum fuzzy entropy principle was employed to determine the membership function parameters. Thirdly, edge information and textural information were extracted to characterize the lesions' features. Scattering phenomenon is a main characteristic of ultrasound images and occurs when tissues are rough or smaller than the scale of the wavelength.

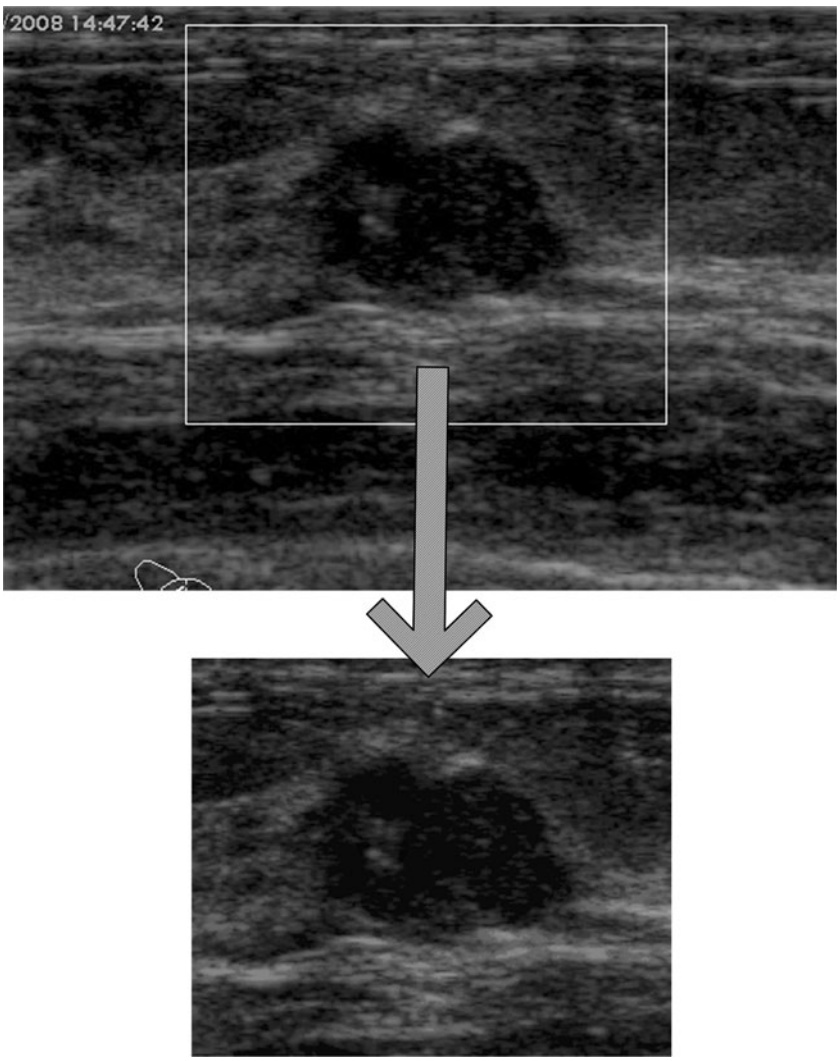

Fig 1. A *rectangular* ROI is manually selected by a radiologist.

The Laws' texture energy measures are used to determine the textural properties of the ROIs in the fuzzy domain.[15,16] The masks are used to depict the edge and spot features of the scattering that are derived from the five vectors.[17] Finally, the local information was used to define the enhancement criterion and contrast ratio, and the images were enhanced by modifying the contrast ratio using both the local and global fuzzy information.

Segmentation

The segmentation of the BUS images utilizes a novel level set-based active contour model. The energy function of the model can be written as the following:

$$E(C) = \alpha \cdot E_C(C) + \beta \cdot E_R(C) + \gamma \cdot E_B(C) \quad (1)$$

Where C is the boundary between different regions, E_{C} (C) is a regularizing term for controlling the length of the boundary curve, E_{R} (C) is a region-based term for considering the global information of the image, and E_{B} (C) is a edge-based term for considering the local information of the image. α, β, and γ are positive constants.

Region-Based Term

Consider image I_{ori} as a real positive function defined in a domain $\Omega \subset R^2$, and the inner and outer regions determined by C are defined as Ω_i and Ω_e. Suppose the intensity distributions of both regions have a prior form, and the distributions can be estimated by using the actual intensities of the two regions. Then, we can define the actual intensity distributions of Ω_i and Ω_e as P_i and P_e and define the estimated intensity probability distributions of Ω_i and Ω_e as P_i^E and P_e^E.

Define the difference measure between the actual and the estimated probability distributions as $D(P, P^E)$, the region-based term can be defined as the total weighted differences between the actual and the estimated intensity probability distributions of Ω_i and Ω_e:

$$\begin{aligned} E_R(C) &= A_i \cdot D\left(P_i, P_i^E\right) + A_e \cdot D\left(P_e, P_e^E\right), \\ D\left(P, P^E\right) &= \sum_{i=0}^{255} \left(P(i) - P^E(i)\right)^2 \end{aligned} \tag{2}$$

where A_i and A_e are the areas of the inner and outer region. Here, the intensity distributions of different tissues are considered as Rayleigh distributions with different parameters σ^2:[18]

$$P_{Rayleigh}\left(I, \sigma^2\right) = \left(I/\sigma^2\right) \cdot \exp\left(-I^2/2\sigma^2\right) \tag{3}$$

The estimated intensity probability distributions can be calculated by maximum likelihood method.

Edge-Based Term

The edge-based term are defined as:

$$E_B(C) = \gamma_1 \cdot \int_C g(x,y)dxdy + \gamma_2 \cdot \int_{\Omega_i} g(x,y)dxdy \tag{4}$$

where γ_1 and γ_2 are constants, and $g(x, y)$ is the edge indicator which can be calculated as the following:

$$g(x,y) = \frac{1}{1 + \left|\nabla G_\sigma(x,y) \times I_{pre}(x,y)\right|^2} \tag{5}$$

where $G_\sigma(\cdot)$is the Gaussian kernel, and I_{pre} can be obtained by pre-processing the original BUS image I_{ori}. The pre-processing is operated in two steps: (1) the image is de-noised by a novel ultrasound de-noising method[19] and (2) the de-noised image is fuzzified for enhancing the contrast.[20]

Regularizing Term

For preventing over-segmentation, the length of the boundary curve is also introduced into the energy function, and it can be written as:[21]

$$E_B(C) = \int_C dxdy \tag{6}$$

Level Set Implementation

To find the minimum of Eq. 1 using the level set method, a level set function ϕ: $(0, \infty) \times \Omega \rightarrow R$ can be introduced into Eq. 1. Let Ω_i be the set $\{(x, y)|\phi(x, y) > 0, (x, y) \in \Omega\}$, and Ω_e be the set $\{(x, y)|\phi(x, y) < 0, (x, y) \in \Omega\}$, then the boundary C can be defined implicitly by the zero level set of ϕ.

Then the energy function can be rewritten as the following:

$$\begin{aligned} E(\Omega_i, \Omega_e) = {} & \alpha \cdot \int_\Omega |\nabla H(\phi(x,y))| dxdy \\ & + \beta \cdot \iint_\Omega \left(p_i - p_i^E\right)^2 H(\phi(x,y)) dxdy \\ & + \beta \cdot \iint_\Omega \left(p_e - p_e^E\right)^2 (1 - H(\phi(x,y))) dxdy \\ & + \gamma \cdot \int_\Omega g(x,y)(\gamma_1 |\nabla H(\phi(x,y))| + \gamma_2 H(\phi(x,y))) dxdy \end{aligned} \tag{7}$$

And the gradient flow can be derived:

$$\begin{aligned} \frac{\partial \phi}{\partial t} &= \delta(\phi) \left[\begin{array}{c} (\alpha + \gamma\gamma_1 g) \operatorname{div}\left(\frac{\nabla \phi}{|\nabla \phi|}\right) - \beta \cdot \left(p_i - p_i^E\right)^2 \\ + \beta \cdot \left(p_e - p_e^E\right)^2 - \gamma\gamma_2 g \end{array} \right] \\ \phi(0, x, y) &= \phi^0(x, y) \text{ in } \Omega \end{aligned} \tag{8}$$

where ϕ^0 is the initial level set function.

Finally, the steps of the proposed algorithm are:

- Initialize the level set function ϕ by ϕ^0
- Compute the actual and estimated probability distributions of the inner and outer regions
- Update ϕ^{n+1} from ϕ^n
- Check the convergence of ϕ; if it still does not reach the steady state, continue the evolution.

After segmentation, the boundary of the breast tumor, C, can be determined. And combining the boundary C and the enhanced image, the result image, I_{res}, can be created as:

$$I_{\text{res}}(x,y) = \begin{cases} 255, & (x,y) \in C \\ I_{\text{en}}(x,y), & (x,y) \notin C \end{cases}$$

All the images in our database were processed by the proposed algorithms. The original and the processed images of each case were saved in separated folders.

Observer Study

Five breast radiologists with varied experience in breast US (range 5 months to 19 years) blinded to the image acquisition procedure analyzed all the cases independently. Three of the radiologists were residents, and the other two radiologists had 10 and 19 years experience in breast US, respectively. All the 226 cases were divided into two groups (groups 1 and 2) randomly; each group has the original and the corresponding processed images. At the first reading section, group 1 was presented to the radiologists with the original and then with the processed images; this design is to simulate clinical use. Radiologists interpret the case first without CAD, give a decision, then read processed images, and revise if they choose to. In this section, cases in group 2 only provided with processed images to analyze the performance of radiologists single with processed images. In order to reduce the bias from memory effect, the second reading section began 2 months later; the cases in both groups were reordered, respectively, i.e., group 1 simply with the processed images and group 2 with the original and then with the processed images presented to the radiologists. Each observer should interpret the cases three times, once with the processed images (observation C), once with the original images (observation A), and then with the both (observation B). The knowledge of clinical history and histological results were not available to the observers during the evaluation.

Before participating the study, all the five radiologists were presented a sheet of the fourth edition of BI-RADS lexicon for sonography;[4] all the observers were familiar with the descriptors during their daily work, and no formal training to the readers were involved in this study. Observers first interpreted each lesion according to sonographic BI-RADS lexicon. And then, the cases were assigned into a BI-RADS final assessment category to indicate the probability of malignancy, including the new subcategories of BI-RADS category 4. In this study, final categories (3, 4a, 4b, 4c, and 5) were corresponding to five classes: benign (category 3), small (category 4a), moderate (category 4b), or substantial (category 4c) likelihood of malignancy and malignant (category 5).

The radiologists made diagnoses according to the following criteria: Lesions displaying all of the signs suggestive of a benign lesion were assigned to BI-RADS category 3 (oval or round shape, parallel orientation, circumscribed margins, abrupt interface, enhancement or absence of posterior acoustic features, absence of surrounding tissue alterations). All lesions exhibiting a combination of at least three signs suggestive of malignancy were assigned to BI-RADS category 5 (irregular shape, nonparallel orientation, echogenic halo, posterior acoustic shadowing, and abnormalities of the surrounding tissue regardless of echo pattern).[4–6] Lesions were assigned to category 4 if they did not meet the requirements for benignity and did not show the combination of at least three suspicious signs, therefore, having indeterminate appearance. Determination of subcategories 4a, 4b, and 4c use the criteria described in the references.[4–6]

Statistical Analysis

A receiver operating characteristic (ROC) analysis was applied to assess the diagnostic accuracy of the radiologists at three conditions (with the processed images, the original images, and then the both). Sensitivity and specificity of readers' classification were calculated. The average area under ROC curve (A_z) was also tested. Difference of US features description between the two analyses with original (observation A) and processed images (observation C) were compared by Chi-square test. P value less than 0.05 was considered to indicate a statistically significant difference. Statistical analyses other than A_z comparison were performed with SPSS for Windows software (version 11.5, Chicago, IL, USA). Medcalc statistical software (Version 8.0.1.0

Schoonjans, Frank) was employed to make A_z comparison.[22]

RESULTS

Features

Two examples of the proposed CAD method are shown in Figures 2 and 3. It can be seen that after enhancement (Figs. 2b and 3b), the internal echo can be displayed better, the microcalcifications were clearer, and the margins are more distinct; the segmentation results help the radiologists to correctly judge the shapes, the margin features, and the orientations of the masses (Figs. 2c and 3c). The final results of the proposed CAD method are shown in Figures 2d and 3d.

The comparative results of all the radiologists' assessments single with and without CAD were listed in Table 1. A total of 226 cases were interpreted using the BI-RADS lexicon for US by five readers; of the seven characters, the descriptors of margin, boundary, and calcification were statistically different for the assessment in observation A versus observation C. Higher rates in spiculated, echogenic hole and microcalcifications were achieved using the processed images. Other features (shape, orientation, echo pattern, post-acoustic features) were not significantly changed by using CAD algorithms.

ROC Analysis

The performance of radiologists in terms of the area under the receiver operating characteristic curve (A_z) was shown in Figure 4 and Table 2, respectively. For the three-time evaluations (observations A, B, and C), observation A (evaluation with the original images) has the lowest diagnosis rate (ranged from 0.772 to 0.846, average 0.810), and observation B (evaluation with processed images aid) has the

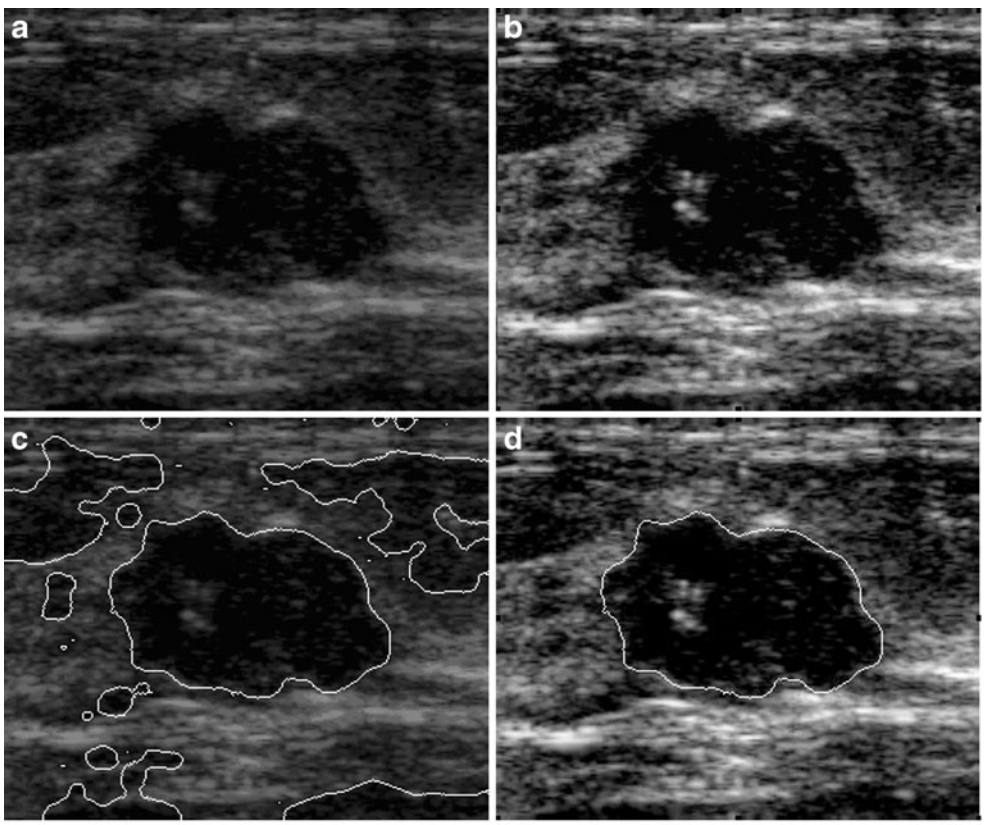

Fig 2. Compared with the original US image (a), the microcalcifications of lesion in the enhanced image (b) are more obvious, and the border of the mass is well delineated in the segmentation image (c). In the resulted image (d), both enhancement and segmentation results are displayed.

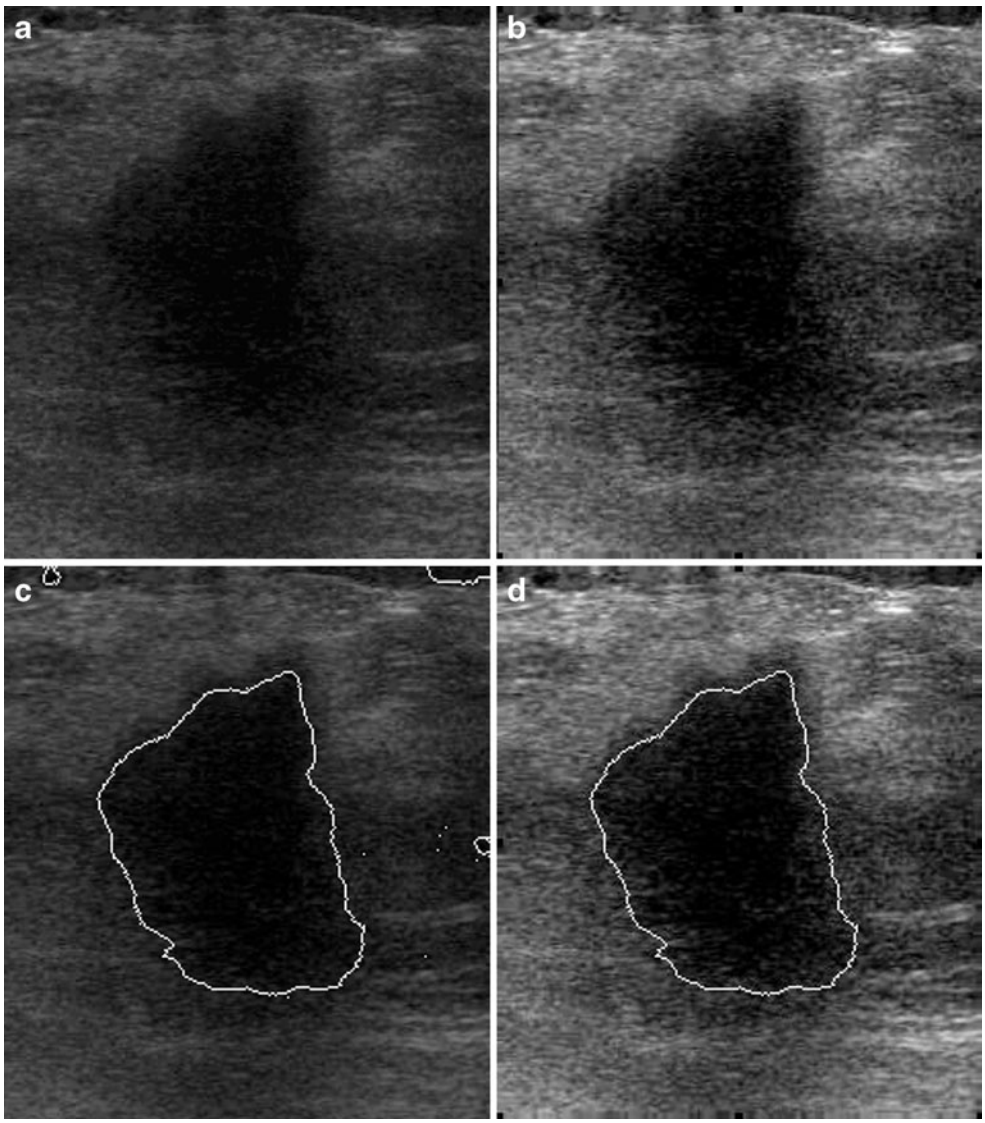

Fig 3. The original image showed a lesion with indeterminate shape and border (a). After enhancement, the lesions became more prominent (b). The segmentation results(c) are quite satisfactory and allow a precise analysis of the shape and margin of the nodule. The result of the proposed CAD method combined by the enhancement and segmentation methods was shown in (d).

highest diagnosis rate (ranged from 0.866 to 0.903, average 0.878); the difference is statistically significant ($p<0.001$). Additionally, performance of observation C (evaluation only use the processed images) is also better than observation A; difference of average A_z is statistically significant ($p<0.001$). Otherwise, the diagnostic rate of observation B is generally higher than observer C, but the different is not significant.

Among the five readers, Radiologist 1 obtained the largest A_z value improvement when reading with CAD; the A_z value for this radiologist was 0.772 without CAD and 0.866 with CAD. The accuracy of this radiology resident with CAD was comparable or slightly superior to that of the experienced radiologist (0.856). Compared with observation A, the improvement of observation C in A_z values were statistically significant for three of five radiologists ($p<0.001$), and the accuracy of the other two experienced radiologists (radiologists 1 and 2) were also improved, but neither of the improvements in A_z values was statistically significant ($p=0.105$ and $p=0.242$, respectively); for observation B, performance

Table 1. Comparisons Without and With CAD in BI-RADS Descriptors

BI-RADS lexicon for US	Descriptors	Sum case (%)		*P* value
		Observation A	Observation C	
Shape	Oval	429 (38.0)	451 (39.9)	0.580
	Round	140 (12.4)	142 (12.6)	
	Irregular	561 (49.6)	537 (47.5)	
Orientation	Parallel	749 (66.3)	728 (62.7)	0.353
	Not parallel	381 (33.7)	402 (37.3)	
Margin	Circumscribed	521 (46.1)	537 (47.5)	0.000
	Indistinct	260 (23.0)	186 (16.5)	
	Angular	108 (9.6)	73 (6.5)	
	Microlobulated	150 (13.3)	195 (17.3)	
	Spiculated	91 (8.1)	139 (12.3)	
Boundary	Abrupt interface	1,024 (90.6)	985 (87.2)	0.009
	Echogenic halo	106 (9.4)	145 (12.8)	
Echo pattern	Anechoic	0 (0.0)	0 (0.0)	0.496
	Hyperechoic	2 (0.2)	2 (0.2)	
	Complex	37 (3.3)	49 (4.3)	
	Hypoechoic	1,087 (96.2)	1,077 (95.3)	
	Isoechoic	4 (0.4)	2 (0.2)	
Posterior acoustic features	Absent	367 (32.5)	355 (31.4)	0.086
	Enhancement	341 (30.2)	368 (32.6)	
	Shadowing	235 (20.8)	258 (22.8)	
	Combined	187 (16.5)	149 (13.2)	
Calcification	Absent	736 (65.1)	621 (55.4)	0.000
	Macrocalcifications	167 (14.8)	159 (14.1)	
	Microcalcifications in mass	118 (10.4)	206 (28.4)	
	Microcalcifications out of mass	109 (9.7)	134 (11.9)	

Observation A shows the data of interpretations using the original images. Observation C shows the data of interpretations using the processed images

of all the five radiologists were statistically improved ($p<0.001$or $p<0.05$).

Accuracy

All the results suggested that when the categories 3 and 4a were diagnosed as negative and categories 4b, 4c, and 5 were diagnosed as positive, the highest accuracy (minimal false negative and false positive results) would be achieved. The sensitivity and specificity of radiologists in classification of masses were clearly shown in Figure 5. For most of the radiologists, the two performance indices were in upward tendency among observations A, C, and B, and both of the indices were improved as the computer aid was used. On the basis of pre-CAD interpretations, the average sensitivity and specificity of radiologists' classification were 80.27% and 69.60%. After CAD image was reviewed, the indices rose to 88.61% and 74.71%. Additionally, observation C had an average sensitivity of 86.90% and specificity of 70.79%. Compared with this perform-

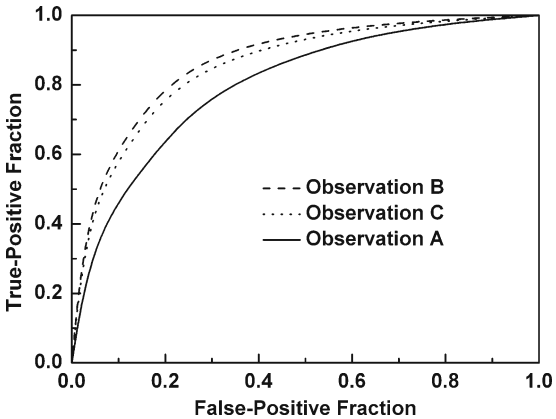

Fig 4. Graph shows the average ROC curves of *observations A, B,* and *C*. *Observation A* represents evaluation only using the conventional images. *Observation B* represents evaluation after reviewing the processed images. *Observation C* represents evaluation only using the processed images.

Table 2. A_z Values for Radiologists in Masses Classification at Three Reading Courses

	Observation A		Observation B		Observation C			
Reader No.	A_z	95%CI	A_z	95%CI	A_z	95%CI	*P* value[a]	*P* value[b]
1	0.772 ± 0.031	0.712~0.825	0.866 ± 0.024	0.815~0.908	0.863 ± 0.024	0.811~0.905	0.000	0.000
2	0.807 ± 0.029	0.749~0.856	0.885 ± 0.022	0.836~0.924	0.867 ± 0.024	0.816~0.909	0.001	0.000
3	0.796 ± 0.030	0.737~0.846	0.872 ± 0.024	0.821~0.913	0.859 ± 0.025	0.807~0.902	0.000	0.000
4	0.828 ± 0.028	0.773~0.875	0.894 ± 0.022	0.846~0.931	0.868 ± 0.024	0.817~0.909	0.242	0.013
5	0.846 ± 0.026	0.792~0.891	0.903 ± 0.021	0.856~0.938	0.878 ± 0.023	0.828~0.918	0.105	0.018
Average	0.810 ± 0.013	0.875~0.835	0.878 ± 0.010	0.857~0.896	0.863 ± 0.011	0.842~0.884	0.000	0.000

Observation A represents evaluation only using the conventional images. Observation B represents evaluation after reviewing the processed images. Observation C represents evaluation only using the processed images. Difference between observation B and C is not significant ($p>0.05$)

[a]Difference between observations A and C

[b]Difference between observations A and B

ance, specificity of observation B was further increased, but sensitivity change was not significant.

DISCUSSION

Computer-aided diagnosis of radiological images has become a rapidly expanding field of research, but its efficacy still needs further validation by clinical trails. In this study, the CAD algorithms including enhancement and segmentation were examined. One of the advantages in this study is using both clinical (observation B) and laboratory experiment (observation C) for evaluation. The confounding bias of repeat reading and memory were excluded. As the results illustrated, observation C is to simply evaluate the performance of the proposed CAD algorithms. Observation B yields better accuracy results than observation C; in another words, combined usage of the original and processed images produced a better performance.

Additionally, accuracy data indicate that the increment in the sensitivity and specificity of the two observation sets were not homogeneous. Assessments using the processed images show significant increase in sensitivity, and specificity improvement was not obvious. In observation B, both kinds of images were employed, and not only the sensitivity but also the specificity were increased. The results of this study suggested that CAD algorithms show advantage in displaying the texture and margin features of the mass and provide more information to the readers, but to avoid missing diagnosis of breast cancer, it always leads to a higher false-positive rate in diagno-

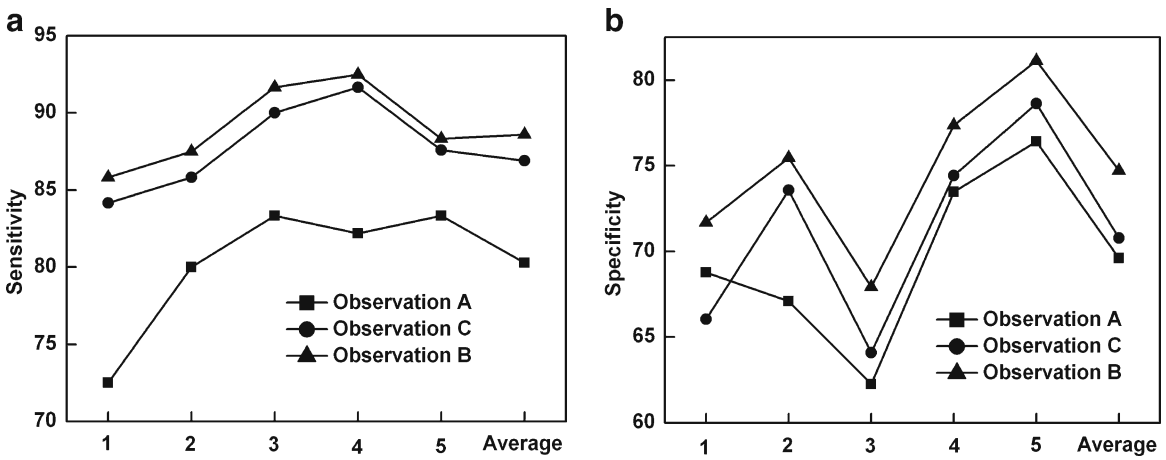

Fig 5. Accuracy indices of the five radiologists and their average performance in the three reading course: a sensitivity of classification, b the corresponding specificity. *Numbers in horizontal axis* represent the five radiologists, respectively.

sis.[23,24] For presence of microcalcifications in the mass is one of the malignant signs; the enhancement algorithm enhanced the texture of the mass and made the microcalcifications more obvious. This improvement helps the readers to increase their diagnosis sensitivity. But for a few benign cases, the microcalcifications can also appear; since the cost of misdiagnose for a malignant lesion is much greater than that for a benign lesion, readers are advised to make a positive rating when they observe the microcalcifications. However, other feature improvements such as distinct margin help increase diagnosis specificity; the condition mentioned above may partly lower the general improvement in specificity. Radiologists' experience and confidence may be responsible for lesion analysis and the final interpretation of an examination.

There are several limitations to our study. No formal training for BI-RADS lexicons was employed in this study; Berg et al.[25] reported that BI-RADS training will result in improved agreement, but the observers in this study were familiar to the descriptors in their daily work.

Another disadvantage is the retrospective nature of the analysis. For all cases involved in our dataset were confirmed by pathological examination, the proportion of malignant cases (53.1%) far exceeds that in daily practice. Although the prevalence of cancer in the dataset was not disclosed to the observer, higher prevalence of malignant cases would cause an increase in sensitivity. However, with the same dataset, the trend of the sensitivity among reading sections is similar.

In conclusion, the study demonstrated that the proposed CAD has great potential in distinguishing malignant from benign breast masses. Combined usage of the original and processed images is better than to use them separately.

ACKNOWLEDGEMENT

Financial support from the National Natural Science Foundation of China (NSFC) is greatly appreciated; grant numbers: 30670546 and 60873142.

REFERENCES

1. Jemal A, Siegel R, Ward E, Hao Y, Xu J, Murray T, Thun MJ: Cancer statistics, 2008. Cancer J Clin 58:71–96, 2008

2. Smigal C, Jemal A, Ward E, Cokkinides V, Smith R, Howe HL, Thun M: Trends in breast cancer by race and ethnicity: update 2006. CA Cancer J Clin 56:168–183, 2006

3. Rajkumar SV, Hartmann LC: Screening mammography in women aged 40–49 years. Medicine 78:410–416, 1999

4. American College of Radiology: Breast Imaging Reporting and Data System (BI-RADS), Ultrasound, 4th edition. Reston: American College of Radiology, 2003 Available at: http://www.acr.org/s_acr/sec.asp?CID =882&DID=14550. Accessed September 8, 2004

5. Hong AS, Rosen EL, Soo MS, Baker JA: BI-RADS for sonography: positive and negative predictive values of sonographic features. Am J Roentgenol 184:1260–1265, 2005

6. Costantini M, Belli P, Ierardi C, Franceschini G, La Torre G, Bonomo L: Solid breast mass characterisation: use of the sonographic BI-RADS classification. Radiol Med 112:877–894, 2007

7. Sehgal CM, Cary TW, Kangas SA, Weinstein SP, Schultz SM, Arger PH, Conant EF: Computer-based margin analysis of breast sonography for differentiating malignant and benign masses. J Ultrasound Med 23:1201–1209, 2004

8. Shen W, Chang R, Moon W, Chou Y, Huang C: Breast ultrasound computer-aided diagnosis using BI-RADS features. Acad Radiol 14:928–939, 2007

9. Chen CM, Chou YH, Han KC, Hung GS, Tiu CM, Chiou HJ, Chiou SY: Breast lesions on sonograms: computer-aided diagnosis with nearly setting-independent features and artificial neural networks. Radiology 226:504–514, 2003

10. Huang YL, Chen DR, Jiang YR, Kuo SJ, Wu HK, Moon WK: Computer-aided diagnosis using morphological features for classifying breast lesions on ultrasound. Ultrasound Obstet Gynecol 32:565–572, 2008

11. Sahiner B, Chan HP, Roubidoux MA, Hadjiiski LM, Helvie MA, Paramagul C, Bailey J, Nees AV, Blane C: Malignant and benign breast masses on 3D US volumetric images: effect of computer-aided diagnosis on radiologist accuracy. Radiology 242:716–724, 2007

12. Chen DR, Chang RF, Chen WM, Moon WK: Computer-aided diagnosis for 3-dimensional breast ultrasonography. Arch Surg 138:296–302, 2003

13. Jackson VP: The role of US in breast imaging. Radiology 177:305–311, 1990

14. Pal SK, Majumder DKD: Fuzzy Mathematical Approach to Pattern Recognition, New York: Wiley, 1986

15. Wu CM, Chen YC, Hsieh KS: Texture features for classification of ultrasonic liver images. IEEE Trans Med Imag 11:141–152, 1992

16. Laws KI: Texture Energy Measures. DARPA Image Understanding Workshop. Los Angeles, CA. 1979, pp 47–51

17. Guo Y, Cheng H-D, Huang J, Tian JW, Zhao W, Sun L, Su Y: Breast Ultrasound images enhancement using fuzzy logic. Ultrasound Med Biol 32:237–247, 2006

18. Wagner RF, Smith SW, Sandrik JM, Lopez H: Statistics of speckle in ultrasound B-scans. IEEE Trans Sonics Ultrason 30:156–163, 1983

19. Guo YH, Cheng HD, Tian JW, Zhang YT: A Novel approach to speckle reduction and its application to ultrasound medical images. Ultrasound Med Biol 35:628–640, 2009

20. Cheng HD, Li JG: Fuzzy homogeneity and scale space approach to color image segmentation. Pattern Recogn 35:373–393, 2002

21. Chan TF, Vese LA: Active contours without edges. IEEE Trans Image Process 10:266–277, 2001

22. Schoonjans F, Zalata A, Depuydt CE, Comhaire FH: MedCalc: a new computer program for medical statistics. Comput Methods Programs Biomed 48:257–262, 1995

23. Krupinski EA: Computer-aided detection in clinical environment: benefits and challenges for radiologists. Radiology 231:7–9, 2004

24. Gilbert FJ, Astley SM, McGee MA, Gillan MGC, Boggis CRM, Griffiths PM: Single reading with computer-aided detection and double reading of screening mammograms in the United Kingdom National Breast Screening Program. Radiology 241(1):47–53, 2006

25. Berg WA, D'Orsi CJ, Jackson VP, Bassett LW, Beam CA, Lewis RS, Crewson PE: Does training in the breast imaging reporting and data system (BI-RADS) improve biopsy recommendations or feature analysis agreement with experienced breast imagers at mammography? Radiology 224:871–880, 2002